Electronic Supplementary Material (ESI) for Journal of Materials Chemistry A.

Insights into Chemical Doping to Engineer the Carbon Nanotube / Silicon Photovoltaic Heterojunction Interface

L. Yu,[1] T. Grace,[1] M. Batmunkh,[1] M. Dadkhah,[1] C. Shearer,[1] and J. Shapter[1,*]

[1]Centre for Nanoscale Science and Technology, School of Chemical and Physical Sciences, Flinders University, Bedford Park, South Australia 5042 (Australia)

Corresponding author: E-mail: joe.shapter@flinders.edu.au

1. Shifting of Fermi level of doping

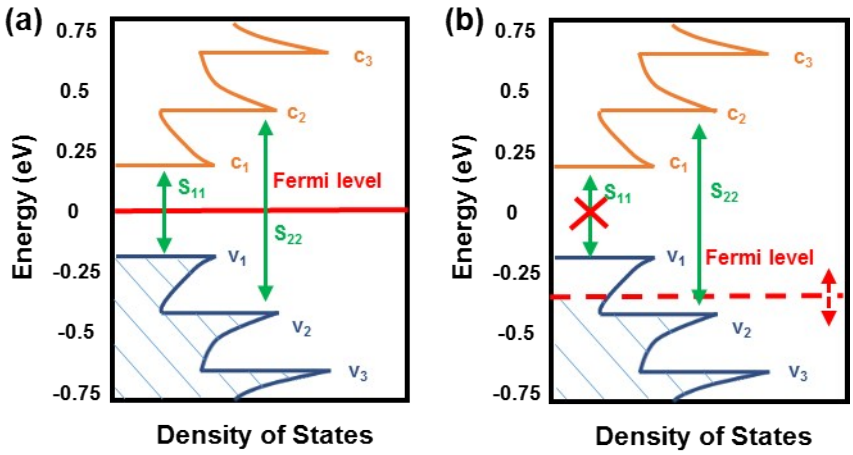

Figure S1 The influence of the p-type dopant on the shifting of Fermi level to the valence band. (a) before and (b) after doping. The solid and short dashed red lines represent the Fermi level before and after doping. C_1, C_2, C_3, V_1, V_2 and V_3 are the first, second and third van Hove singularities in the conduction and valence band. Filled areas show the filled states.

As shown in **Figure S1**, p-type dopants enable the Fermi level shift down towards the valence band, which results in a decreased number of electrons being excited from V_1 to C_1 and thus the optical absorption peak in the lower energy range (S_{11}) is suppressed.

2. Synthesis of GO

A mixture of 40 mL H_3PO_4 (86.5 %, BDH Chemicals) and concentrated 360 mL H_2SO_4 (98.0 %, RCI Labscan) (9:1) was added to the mixture of graphite flakes (Sigma-Aldrich) and $KMnO_4$ (99.0 %, Chem-Supply) (3 g/ 18 g). The reaction was heated at 50 °C for 12 h with stirring. The reactor was then cooled down to room temperature and the liquid was centrifuged at 1800 g for 4 h. The supernatant was discarded and the top 70 % of the solid was collected and rinsed with deionized water (200 mL), 30 % HCl (200 mL) and ethanol (200 mL two times) in succession. After each wash step, the mixture was centrifuged at 4000 rpm for 4 h and the supernatant was disposed while the top 70 % of the solid content was collected for the following wash. The solid was dried in a freeze dryer overnight after the

final wash, and collected as the as prepared GO solids, which were then suspended with deionized water by bath sonication for 20 min with the final concentration to be 1 mg mL^{-1}.

3. Preparation of GOCNT suspension

5 mg CNT (P3-SWNT, Carbon Solutions Inc., USA) were dispersed with 50 mL of deionized water by bath sonication for 1 h. 2 mL GO stock suspension was added into 45 mL CNT dispersion. The GOCNT mixture was further bath-sonicated for 90 min before being centrifuged at 17500 g for 1 hour at 10 °C for removal of large agglomerates. The supernatant was collected and centrifuged again in an identical manner. The second supernatant was collected and stored as the initial suspension for the preparation of GOCNT transparent hybrid electrodes. All the sonication steps in the procedure were conducted within an ice bath.

4. Synthesis and characterization of AgNWs

6 g of polyvinylpyrrolidone (PVP, MW = 55000 g mol^{-1}, Sigma-Aldrich) was dissolved in 190 mL of glycerol (99.5 %, Chem-Supply) at 80 °C. The solution was then cooled down to room temperature and poured into a round-bottom flask in a silicone oil bath, followed by the addition of silver nitrate (1.58 g, AgNO3, 99.0 %, Sigma-Aldrich) with vigorous stirring. Then, 58.5 mg of sodium chloride (NaCl, 99.7 %, Chem-Supply) was dissolved in 0.5 mL water and mixed with 10 mL glycerol. The NaCl solution was loaded into the reactor and the reaction temperature was raised to 205 °C rapidly (within 25 min). The reaction was performed at 205 ± 1 °C for 60 min in air. After the reactor was cooled down to the room temperature, the liquid was mixed with deionized water in a volume ratio of 1 : 1. The mixture was then centrifuged at 4000 g for 5 min at room temperature. The supernatant was disposed of and the collected precipitants were redispersed with water and centrifuged in the same manner three times to remove the PVP and nanoparticles. After a final wash, the AgNWs were suspended in water with the final concentration to be 0.2 mg mL^{-1}.

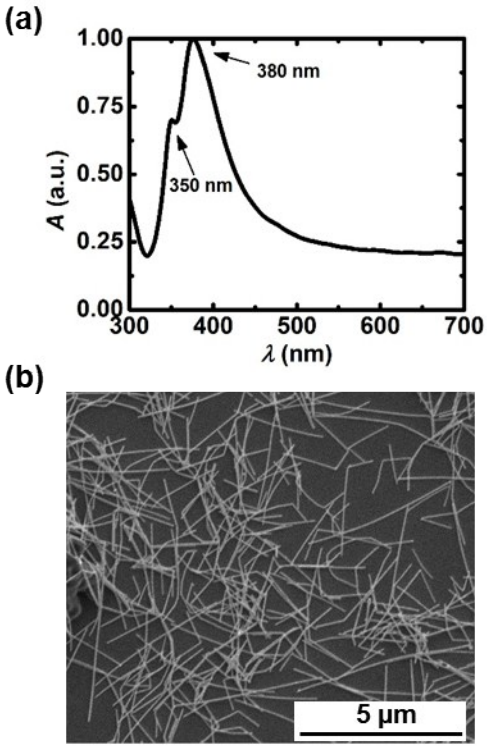

Figure S2: (a) UV-Vis absorbance spectrum of AgNWs aqueous dispersion (normalized at 380 nm) and SEM images of (b) AgNWs on Si surface by drop casting.

As shown in **Figure S2 (a)**, characteristic peaks of AgNWs at 350 and 380 nm are observed in the UVVis spectrum. In addition, **Figure S2 (b)** is an SEM image of the AgNWs on Si, where most of AgNWs have the length of 5 ± 2 μm.

5. Si substrates

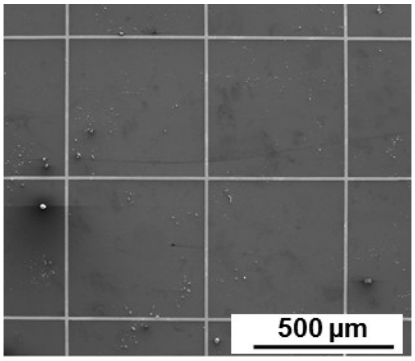

Figure S3: SEM images of Si substrates with the defined grid pattern of front metal electrode.

As shown in **Figure S3**, the line spacing of the grid pattern is 0.5 mm and the line width is 0.01 mm.

6. Calculation of ideality and J_{sat}

Ideality and J_{sat} were calculated from the fitting of the linear parts of the dark J-V curve with **Equation S1** for studying the diode properties.[27]

$$J = J_{Sat}[e^{\frac{qV}{nkT}} - 1] \qquad \textbf{Equation S1}$$

where J is the measured current density under the dark condition; q is elemental charge (1.602×10^{-19} C); V is the applied voltage during the measurement; n is the ideality; k is Boltzmann constant (1.381×10^{-23} m^2 kg s^{-2} K^{-1}) and T is the temperature (293 K).

The Schottky barrier height (ϕ_B) is related to J_{sat} and can be calculated by **Equation S2**:[47]

$$\phi_B = -kT\ ln(\frac{J_{Sat}}{A^* T^2}) \qquad \textbf{Equation S2}$$

where A^* is Richardson constant (112 A cm^{-2} K^{-2} for Si).[48]

7. XPS of CNT and GOCNT films

XPS measurements were collected at the soft x-ray beamline of the Australian synchrotron. Samples were prepared by filtering onto Au/Cr (10 nm, 2 nm) coated alumina filter discs (0.02um pore size, anodisc, Whatman, VWR Australia) and measured without heating. Presented spectra were collected with 850 eV excitation energy which was calibrated from the binding energy Au 4f position of gold foil (84.00 eV). Photoelectrons were analyzed using a Specs electron analyzer and SpecsLab2 Software with survey spectrum collected with pass energy of 20 eV and energy step of 0.5 eV. Higher resolution C1s spectra were collected with pass energy of 5 eV and energy step of 0.05 eV.

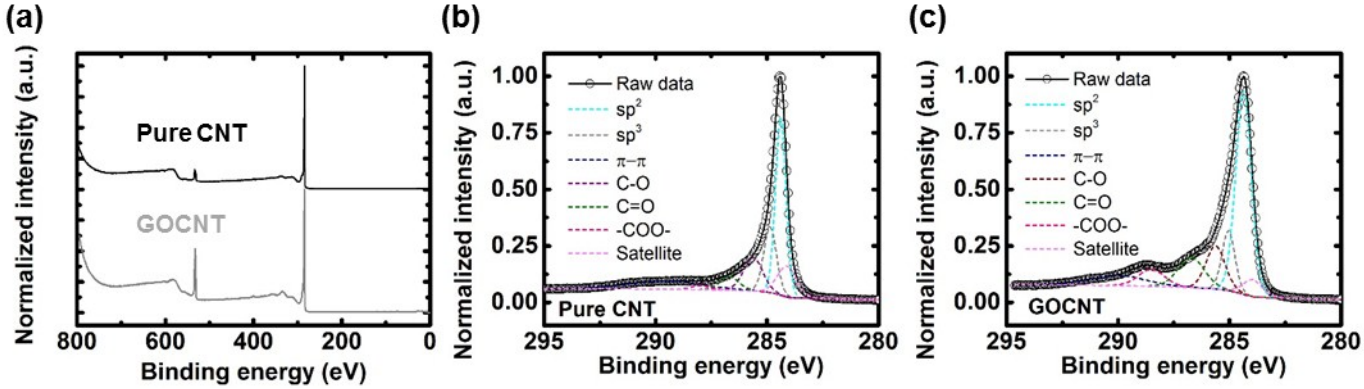

Figure S4 (a) XPS specta of CNT and GOCNT films, fitting of C 1s peak for (b) pure CNT and (c) GOCNT films.

As shown in **Figure S4**, GOCNT film has a higher signal intensity of oxygen compared to that of pure CNT film, which indicates the existence of GO in the hybrid. The carbon content for pure CNT and GOCNT films are 85 and 68 % respectively (compared to < 50% for GO, data not shown) and it suggests that the main species in the hybrid films are still carbon nanotubes. Fitting of the C 1s spectrum reveals an increase in relative intensity from C=O and -COO- but the main line signal from sp^2 hybridized carbon at ~284.4 eV remains the most intense suggesting that the GOCNT films are dominated by the CNTs.

7. SEM images of the GOCNT films

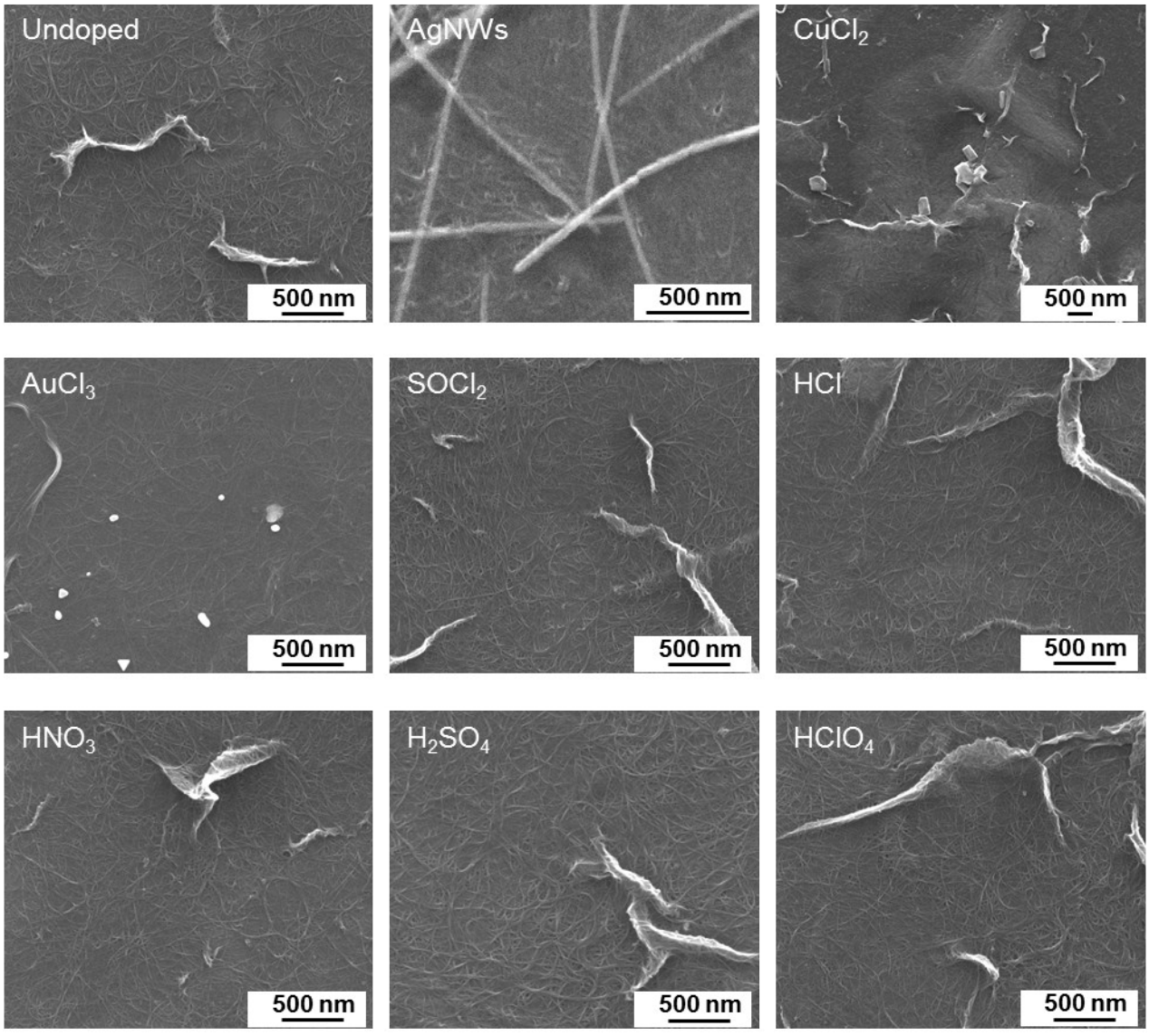

Figure S5: SEM images of GOCNT films before and after different treatments, including AgNWs, $CuCl_2$, $AuCl_3$, $SOCl_2$, HCl, HNO_3, H_2SO_4 and $HClO_4$.

As shown in **Figure S5**, as expected, AgNWs are observed in the AgNWs GOCNT mixture while metal nanoparticles are observed in both $CuCl_2$ and $AuCl_3$ doped films. However, the films after $SOCl_2$, HCl, HNO_3, H_2SO_4 and $HClO_4$ treatment are very similar to the untreated film.

8. Intensity of S_{11}, S_{22} and the averaged of both

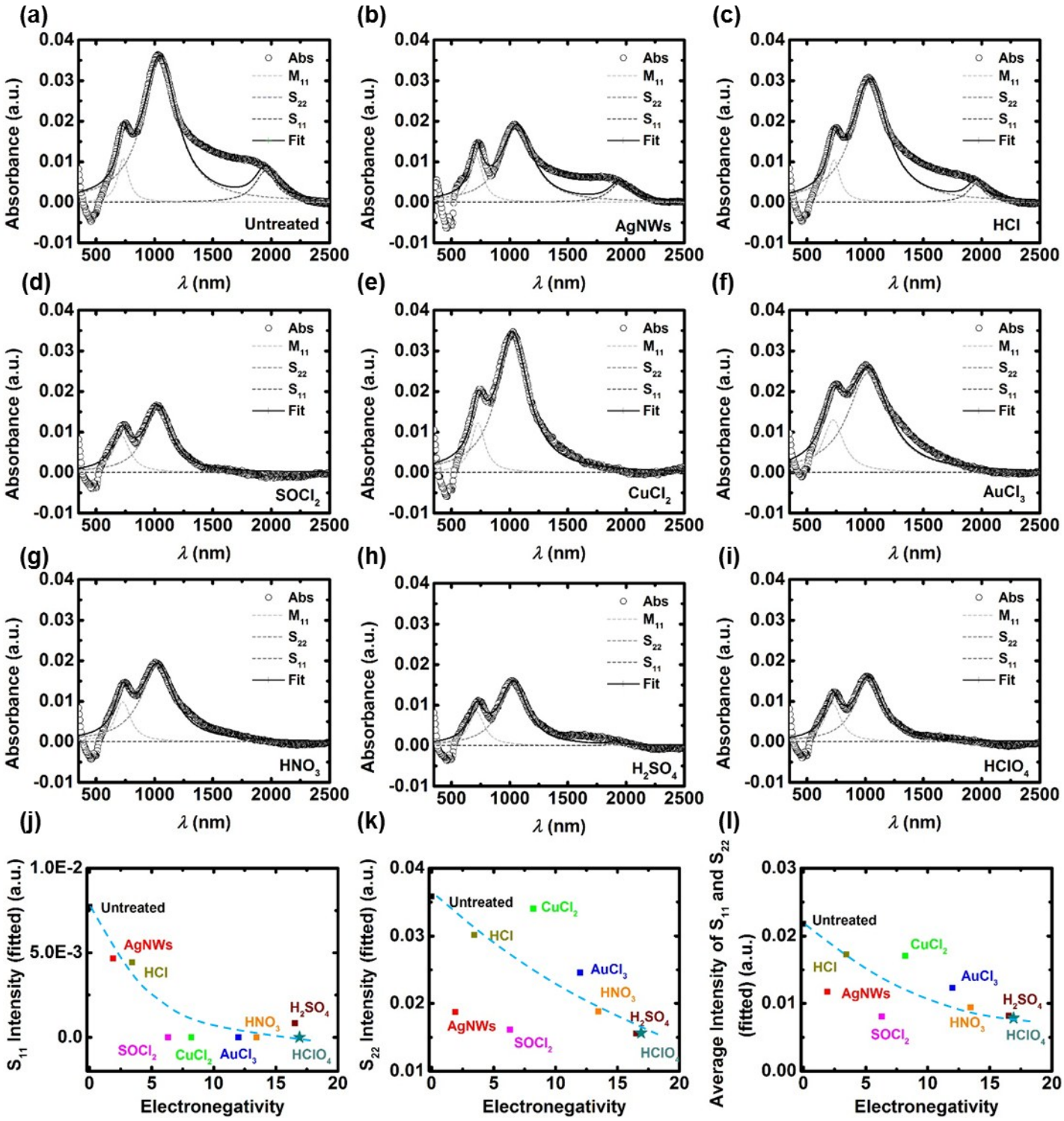

Figure S6 Fitting of UV-Vis-NIR spectra after background subtraction (proposed by Naumov) (a) untreated, (b) AgNWs, (c) HCl, (d) $SOCl_2$, (e) $CuCl_2$, (f) $AuCl_3$, (g) HNO_3, (h) H_2SO_4 and (i) $HClO_4$; Intensity of (j) S_{11}, (k) S_{22} and (l) the averaged intensity of S_{11} and S_{22} in the UV-Vis-NIR spectra as a function of electronegativity for GOCNT films. The trend lines in the figures are added to guide the eye.

As shown in **Figure S6 (a)-(i)**, the UV-Vis-NIR spectra are fitted with three Lorentzian peaks (S_{11}, S_{22}, and M_{11}) after background subtraction. The intensity of both S_{11} and S_{22} peaks (and the average values of S_{11} and S_{22}) decreases with the electronegativity of different dopants (AgNWs treated GOCNT films does not follow this trend), which is due to the shifting of Fermi level after treatments, as shown in **Figure S6 (j)-(l)**.

9. Fitting of G band of Raman spectra

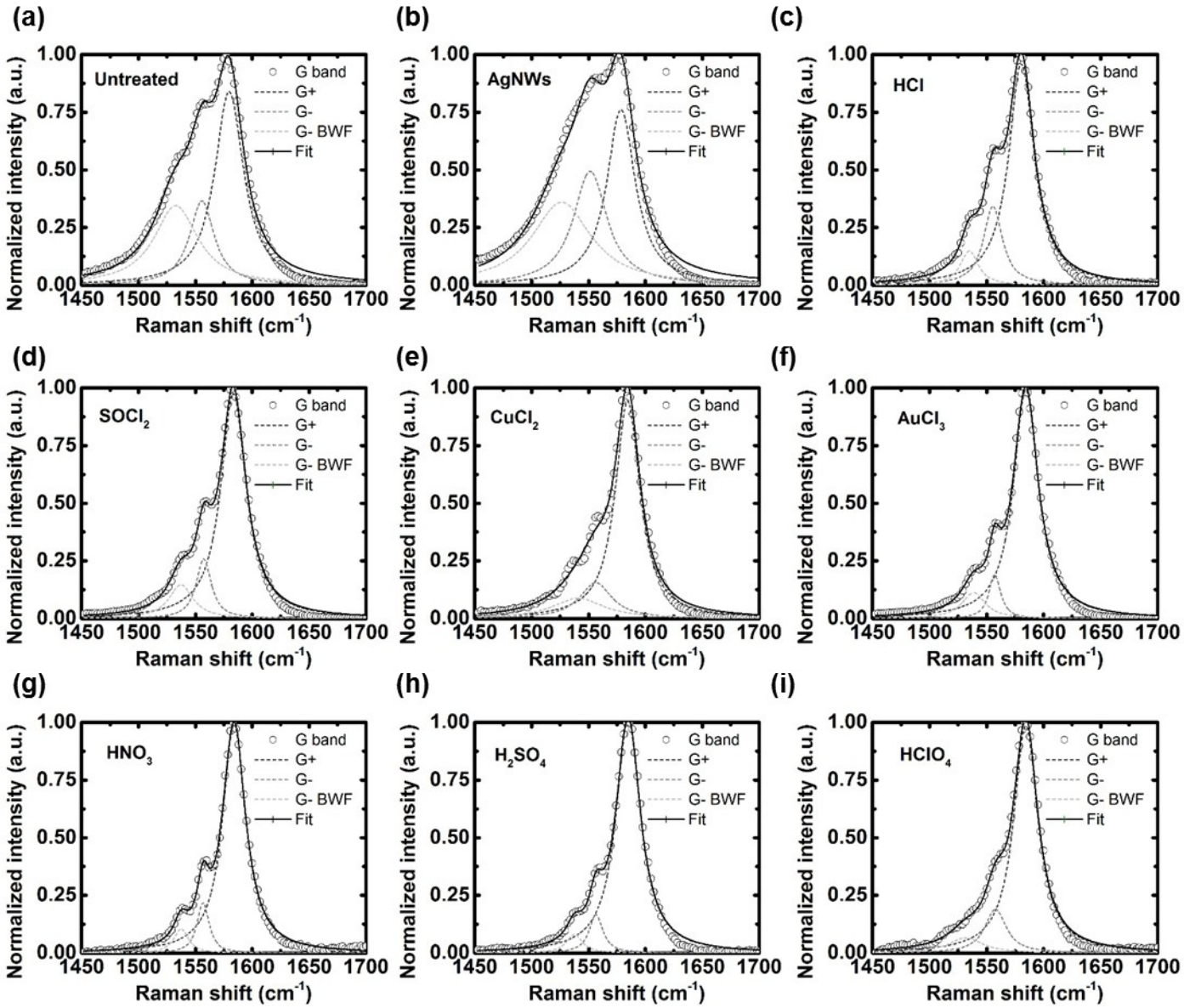

Figure S7: Fitting of Raman G band of GOCNT films treated with different materials, (a) untreated, (b) AgNWs, (c) HCl, (d) $SOCl_2$, (e) $CuCl_2$, (f) $AuCl_3$, (g) HNO_3, (h) H_2SO_4 and (i) $HClO_4$.

As shown in **Figure S7**, Raman spectra are normalized to the peak of the G band which was fit with three different peaks (G^+ Lorentzian, G^- Lorentzian and G^- BWF, from high Raman shift to low Raman shift). BWF is related to metallic species in the film, and it is suppressed to different extents with various p-type dopants while it remains at a similar level in the AgNWs treated sample as that observed for the control film, which is further evidence inferring that AgNWs might not be a p-type dopant.

10. Performance of solar cells

The details of solar cell performance are shown in **Table S1** and **Table S2**, and these data are analyzed in the main text and plotted in **Figure 4**.

Table S1: Details of solar cell performance extracted from *J-V* light curves of GOCNT/Si solar cells with and without different treatments. The errors are the standard deviation of the results of 3 solar cells on each type.

	Efficiency (%)	J_{SC} (mA cm^{-2})	V_{OC} (V)	*FF*	R_{shunt} (Ω)	R_{series} (Ω)
Untreated	7.11 ± 0.35	26.20 ± 0.23	0.546 ± 0.009	0.49 ± 0.01	$2.38 \times 10^3 \pm 6.58 \times 10^2$	92 ±4
AgNWs	8.14 ± 0.27	26.07 ± 0.31	0.557 ± 0.014	0.56 ± 0.01	$7.40 \times 10^3 \pm 1.26 \times 10^3$	113 ±5
$CuCl_2$	10.12 ± 0.33	26.21 ± 0.27	0.584 ± 0.006	0.66 ± 0.01	$1.48 \times 10^5 \pm 2.35 \times 10^3$	66 ±3
$AuCl_3$	10.07 ± 0.31	26.14 ± 0.32	0.566 ± 0.016	0.68 ± 0.01	$1.55 \times 10^5 \pm 3.66 \times 10^3$	62 ±3
$SOCl_2$	10.26 ± 0.29	26.36 ± 0.42	0.588 ± 0.004	0.66 ± 0.01	$1.42 \times 10^5 \pm 1.86 \times 10^3$	65 ±2
HCl	8.99 ± 0.22	26.13 ± 0.37	0.575 ± 0.004	0.60 ± 0.01	$1.33 \times 10^5 \pm 1.79 \times 10^3$	87 ±3
H_2SO_4	11.02 ± 0.24	26.42 ± 0.21	0.589 ± 0.003	0.71 ± 0.01	$1.96 \times 10^5 \pm 2.65 \times 10^3$	48 ±3
HNO_3	11.38 ± 0.26	26.83 ± 0.19	0.588 ± 0.002	0.72 ± 0.01	$1.97 \times 10^5 \pm 3.10 \times 10^3$	47 ±2
$HClO_4$	11.35 ± 0.32	26.69 ± 0.25	0.590 ± 0.003	0.72 ± 0.01	$2.04 \times 10^5 \pm 2.24 \times 10^3$	46 ±3

Table S2: Details of solar cell performance extracted from *J-V* dark curves of GOCNT/Si solar cells with and without different treatments

	Ideality	J_{Sat} (mA cm^{-2})	ϕ_B (eV)
Untreated	1.71 ± 0.24	$1.97 \times 10^{-5} \pm 3.33 \times 10^{-6}$	0.85 ± 0.01
AgNWs	1.52 ± 0.12	$3.93 \times 10^{-6} \pm 2.98 \times 10^{-6}$	0.90 ± 0.02
$CuCl_2$	1.24 ± 0.07	$1.66 \times 10^{-7} \pm 7.33 \times 10^{-8}$	0.96 ± 0.01
$AuCl_3$	1.38 ± 0.08	$1.71 \times 10^{-6} \pm 1.52 \times 10^{-6}$	0.92 ± 0.02
$SOCl_2$	1.30 ± 0.05	$3.37 \times 10^{-7} \pm 1.61 \times 10^{-7}$	0.96 ± 0.02
HCl	1.41 ± 0.06	$1.36 \times 10^{-6} \pm 9.25 \times 10^{-7}$	0.93 ± 0.03
H_2SO_4	1.21 ± 0.03	$1.60 \times 10^{-7} \pm 1.01 \times 10^{-7}$	0.98 ± 0.01
HNO_3	1.20 ± 0.03	$9.51 \times 10^{-8} \pm 4.87 \times 10^{-8}$	0.99 ± 0.01
$HClO_4$	1.20 ± 0.03	$1.68 \times 10^{-7} \pm 1.33 \times 10^{-7}$	0.98 ± 0.01

11. Integration of EQE curves

As shown in **Table S3**, the calculated J_{SC} are between 26 to 27 mA cm^{-2}, which is the same range as the measure values. In addition, this also suggests that all of the devices have similar J_{SC} no matter what treatment has been performed.

Table S3: The calculated J_{SC} based on the integration of EQE curves

	Calculated J_{SC} (mA cm^{-2})	Measured J_{SC} (mA cm^{-2})
Untreated	26.01	26.20 ± 0.23
AgNWs	26.32	26.07 ± 0.31
$CuCl_2$	26.63	26.21 ± 0.27
$AuCl_3$	26.53	26.14 ± 0.32
$SOCl_2$	26.70	26.36 ± 0.42
HCl	26.80	26.13 ± 0.37
H_2SO_4	26.41	26.42 ± 0.21
HNO_3	26.63	26.83 ± 0.19
$HClO_4$	26.72	26.69 ± 0.25

12. Degradation of solar cells over 10 days

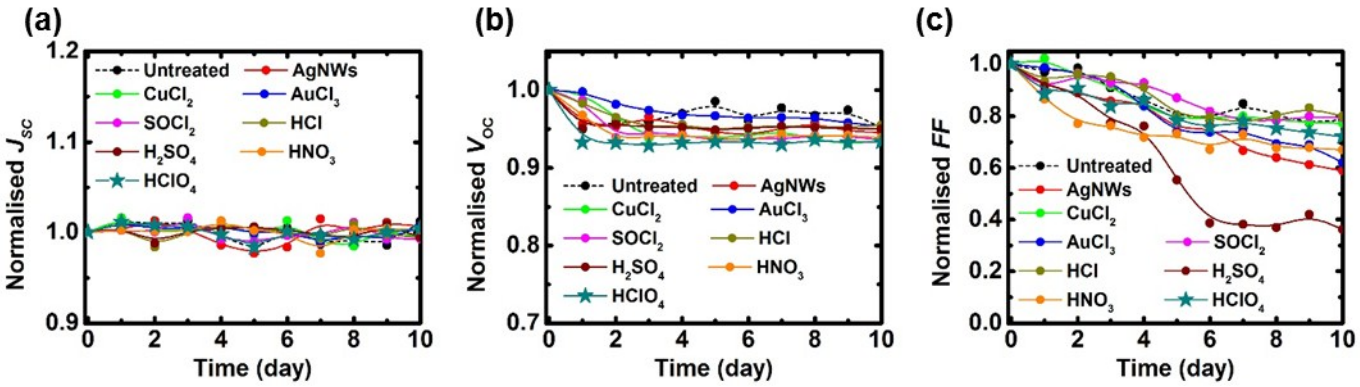

Figure S8: The performance degradation of the solar cells within 10 days (a) J_{SC}, (b) V_{OC} and (c) FF. The trend lines in the figures are added to guide the eye.

As shown in **Figure S7 (a)**, J_{SC} was stable for 10 days for all devices. V_{OC} decreased rapidly in the first 2-3 days and then stayed unchanged while FF decreased continuously over the 10 days, including the untreated devices. This suggests that the growth of oxide layer took place continuously over the 10 days but it does not have a strong influence on V_{OC} after the initial formation of the oxide layer.